The International Journal of Advanced Manufacturing Technology (2023) 128:4207–4221
https://doi.org/10.1007/s00170-023-12181-8

ORIGINAL ARTICLE

Soft pneumatic actuators with integrated resistive sensors enabled by multi-material 3D printing

Mohammadreza Lalegani Dezaki[1] · Rylz Sales[1] · Ali Zolfagharian[2] · Hamed Yazdani Nezhad[3,4] · Mahdi Bodaghi[1]

Received: 8 June 2023 / Accepted: 15 August 2023 / Published online: 29 August 2023

Abstract

The concept of soft robots has garnered significant attention in recent studies due to their unique capability to interact effectively with the surrounding environment. However, as the number of innovative soft pneumatic actuators (SPAs) continues to rise, integrating traditional sensors becomes challenging due to the complex and unrestricted movements exhibited by SPA during their operation. This article explores the importance of utilising one-shot multi-material 3D printing to integrate soft force and bending sensors into SPAs. It highlights the necessity of a well-tuned and robust low-cost fabrication process to ensure the functionality of these sensors over an extended period. Fused deposition modelling (FDM) offers a cost-effective solution for embedding sensors in soft robots, directly addressing such necessity. Also, a finite element method (FEM) based on the nonlinear hyper-elastic constitutive model equipped with experimental input is developed to precisely predict the deformation and tip force of the actuators measured in experiments. The dynamic mechanical test is conducted to observe and analyse the behaviour and resistance changes of conductive thermoplastic polyurethane (CTPU) and varioShore TPU (VTPU) during a cyclic test. The flexible sensor can detect deformations in SPAs through the application of air pressure. Similarly, the force sensor exhibits the ability to detect grasping objects by detecting changes in resistance. These findings suggest that the resistance change corresponds directly to the magnitude of the mechanical stimuli applied. Thus, the device shows potential for functioning as a resistive sensor for soft actuation. Furthermore, these findings highlight the significant potential of 3D and 4D printing technology in one-shot fabrication of soft sensor-actuator robotic systems, suggesting promising applications in various fields like grippers with sensors and rehabilitation devices.

Keywords 3D/4D printing · Multi-material printing · Soft pneumatic actuators · Soft sensors · Fused deposition modelling

1 Introduction

Soft pneumatic actuators (SPAs) function by introducing controlled positive or negative pressure into a sealed chamber within a pliable structure [1]. These actuators can bend, twist, extend, or contract and the motions of SPAs can be monitored through sensors [2]. The response of the actuator to the pressure applied depends on both materials and the configuration of chambers. The geometric shape and distribution of multiple materials in the actuator can be enhanced in a more comprehensive manner. In terms of the autonomous design of soft robots and actuators, optimizing design may prove advantageous [3–5]. Soft actuators provide a safer way to connect with rigid structures due to their pliability, allowing for natural joint movements during rehabilitation. Moreover, sensors assist in tracking the movement and regulating the behaviour of SPAs [6]. SPAs are primarily utilized in the fields of robotics and biomechanics due to their ability to interact with delicate bodies and biological systems [7]. There are methods available for producing SPAs and soft sensors such as 3D printing and casting [8–13]. 3D printing of soft components is a widely adopted manufacturing technology. Fused deposition modelling (FDM) is one of

✉ Mahdi Bodaghi
mahdi.bodaghi@ntu.ac.uk

1 Department of Engineering, School of Science and Technology, Nottingham Trent University, Nottingham NG11 8NS, UK

2 School of Engineering, Deakin University, Geelong 3216, Australia

3 Faculty of Engineering and Physical Sciences, University of Leeds, Leeds LS2 9JT, UK

4 Advanced Composites Research Focused Group, School of Science and Technology, City, University of London, London EC1 0HB, UK

the most utilized 3D printing techniques for producing soft products [14–17].

SPAs with integrated sensors are advanced systems that can adjust their posture, gripping force, and gripping shape based on the characteristics of the object they are grasping [18, 19]. They find extensive usage in a range of applications including medical rehabilitation devices, wearable gadgets, and soft robots [20–23]. SPAs can be fabricated using different materials, but the most common materials are flexible and pliable, such as elastomer and thermoplastic polyurethane (TPU). These materials provide the necessary compliance and flexibility that enable the SPA to deform and generate energy [24, 25]. On the other hand, soft sensors are devices that can detect and measure changes in pressure, strain, or temperature and convert them into electrical signals. Soft sensors are often integrated with SPAs to provide feedback on the deformation and motion of the SPA [26]. To fabricate soft sensors, conductive materials enable electrical signal transmission while electroactive polymers generate signals in response to mechanical deformation or pressure changes [27–30].

There have been studies proposing various designs and advancements of SPAs utilizing 3D printing technology [31, 32]. Tawk et al. [33] utilized an affordable and open-source FDM technique to 3D print the fingers of a soft gripper, along with a mechanical metamaterial incorporating a pliable auxetic structure and compliant ribs. The outcomes revealed that the gripper could effectively grasp a wide range of objects with three different configurations consisting of two, three, and four fingers. Also, Cheng et al. [34] developed centrifugal multi-material 3D printing to create a wide range of multi-material products. The 3D printing system allowed for the direct 3D printing of a SPA with integrated bending, pressure, and temperature sensors. The complete SPA could be produced in a single 3D printing process using five distinct polymers, including a stretchable elastomer, hard polymer, soft polymer, conductive hydrogel, and ionic conductive elastomer. The sensors responded continuously to changes in the actuators' behaviour. Many commercial 3D print materials offer a wide range of flexibility and hardness. Lalegani Dezaki et al. [35] utilized FDM technology along with bio-inspired lattice chambers to create SPAs using varioShore TPU (VTPU) material. This material offers several advantages, including variable shore hardness, density control, and a soft touch, which are highly beneficial for soft robotics applications [36]. The primary objective was to produce the possible softest sample, which held great significance in the field of soft robotics. By adjusting the nozzle temperature and material flow rate, they could change the material density. Also, the goal was to engineer SPAs that exhibited different behaviours for controlling tip deflection and tip force while using the same input air pressure. The study's outcomes show that lattice patterns govern the bending angle and produced force of the actuators. Additionally, these lattices enhance the overall strength by regulating the contact area within the chambers. The research shows that these soft actuators exhibit different stiffness characteristics and deformations under the same pressure levels ranging from 100 to 500 kPa.

Moreover, Gariya et al. [37] used a bending-type SPA that could generate bending energy based on the piezoelectric effect. Their main goal was to create a new type of SPA that incorporates a piezoelectric membrane (SPA-P). The SPA-P was made by combining a flexible conducting polymer nanocomposite membrane with the silicone rubber body of the SPA. SPA-P exhibited a noticeable change in voltage when activated by pneumatic pressure. This voltage change could be used to provide feedback control for the SPA by correlating it with the deformation during bending. Moreover, Hohimer et al. [38] used multi-material FDM to print composites made of flexible TPU and multi-walled carbon nanotubes. The goal was to investigate the possibility of incorporating built-in sensing capabilities into soft robotics. The study successfully demonstrated the built-in sensing capabilities of the printed actuators through capacitive and piezoresistive sensing. These capabilities were shown to work effectively during gripping contact and actuation at different pressure levels. The results suggest that integrating various feedback sensors in robotic actuators through the FDM process has significant potential.

Due to the significant growth in the field of soft robotics and the development of innovative SPAs, traditional soft sensors are inadequate for meeting the diverse range of motion capabilities required for practical applications. Sensors that are highly efficient, such as magnetoelastic and flexible inductive sensors, have specific requirements and tend to be costly. These sensors may also need regular maintenance for their components [39, 40]. External optical sensors, such as custom-made cameras, are an alternative method for monitoring soft actuators. Nevertheless, their practical application may constrain the actuator's motion and demand significant electrical power to operate effectively [41].

The aim of this paper is the development of a cost-effective method for fabricating SPAs with built-in soft force and bending sensors, using multi-material FDM 3D-printing technology. The novelty of this study lies in the utilisation of one-shot multi-material printing to create SPA with integrated force and bending sensors. The objective is to investigate the feasibility of using a conductive material as a sensing element within the SPA, to monitor and control its performance. The addition of such sensors would enhance the SPA's functionality, allowing it to provide more detailed feedback data, which can be used to optimize its behaviour. By using a conductive material that exhibits changes in resistivity as a response to bending and applied force, the SPA can be effectively monitored and controlled. This approach

offers a low-cost and efficient method for incorporating sensing capabilities into soft robotic systems. The topics covered include an exploration of the background of SPAs, considerations for material selection, the process of designing and fabricating these actuators, experimental findings, simulation of SPAs, mechanical properties, potential applications, and future directions for sensory device development.

2 Materials and methods

2.1 Materials

In this study, VTPU material supplied by Colorfabb is used as the main material for SPAs. Also, conductive TPU (CTPU) filaflex from Recreus is used for soft sensors. It is crucial to thoroughly investigate the material properties to achieve the desired softness in soft robotic actuators. The CTPU filament is a flexible filament that possesses electrical conductivity, exhibits electrical resistance, and a shore hardness of 92A [42]. The material is made by incorporating conductive materials, such as carbon black, into the base polymer. The amount and type of conductive material used can vary, affecting the conductivity of the final filament. It is specifically designed for producing electrically conductive parts or components, making it highly suitable for the manufacturing of wearable devices and sensors [43].

2.2 Mechanical properties

In order to gain insights into the mechanical properties of the VTPU and CTPU filament, mechanical testing is conducted on each material separately [44, 45]. The tensile tests allow for the validation of the sensor integrated with the VTPU matrix and a comprehensive understanding of the material's characteristics. The behaviour of VTPU and CTPU is studied by conducting a uniaxial tensile test to analyse its stress-strain relationship. These samples are produced with the same printing parameters and longitudinal infill patterns as mentioned in Table 1. The tensile tests are conducted in accordance with the guidelines outlined in ASTM D412-16 [46], which specifies the standard procedure for evaluating the tensile properties of plastics. During the tests, all the samples are stretched at a controlled rate of 500 mm/min using an electromechanical machine called the Shimadzu AG-X plus. The tensile test data are recorded and analysed using the TRViewX software.

To evaluate the mechanical and electrical behaviour of the sensor, CTPU is printed on the surface of VTPU strips with dimensions of 130 mm x 10 mm x 0.3 mm. The procedure and setup for the test are done based on previous reports to validate the results [24, 26, 47]. To avoid slippage during the tensile testing experiments, clamps are utilized.

Table 1 Printing parameters of CTPU and VTPU

Printing parameters	Material	
	VTPU	CTPU
Bed Temperature (°C)	0	0
Nozzles Temperature (°C)	225	225
Nozzles Diameter (mm)	0.4	0.4
Wall Thickness (mm)	1	1
Infill Density (%)	100	100
Infill Pattern	Zigzag	Concentric
Material Flow (%)	100	100
Print Speed (mm/s)	25	25

The CTPU response of the integrated strain-sensing elements is continuously monitored in real time. Due to the high resistive nature of the printed sensor, a two-terminal sensing mode is employed to examine its resistance. To ascertain the variation in the resistance value, the average result is computed using measurements obtained from three samples. The dynamic characteristics of the materials are examined through the implementation of a cyclic tensile test. This entails subjecting the samples to ten repeated cycles of stretching and releasing to evaluate their performance in dynamic scenarios. In the initial phase, the dynamic performance of the printed VTPU and CTPU strips with integrated sensing elements is assessed by conducting tests at strain levels spanning from 0% to 30% and 0% to 100% at a controlled rate of 200 mm/min. The strain and electrical resistance changes are constantly recorded using TRViewX and LabVIEW to detect changes in resistance while testing is ongoing. The resistance starts to change by applying the tensile load to the strips. Thus, the strain and electrical resistance changes are recorded using TRViewX and Keithley 2110 digital multimeter.

2.3 Design and modelling

The design of SPAs plays a critical role in their performance and functionality. The design affects the overall actuation capabilities and provides housing for essential electrical components like sensors and power supplies. These components can significantly impact the manoeuvrability and operation of the SPAs. Therefore, when developing a functional SPA, it is crucial to consider variables such as the weight and parameters of these components.

Moreover, sensors play a vital role in soft robotics by capturing the position and physical characteristics of soft robots at any given moment. These sensors enable the implementation of a closed-loop system approach, which is utilized to control the infinite degrees of freedom offered by soft actuators. By integrating sensors into the system, real-time feedback on the robot's position and physical state can be

obtained, allowing for precise and responsive control of its movements. In this study, two types of sensors, bending and force sensors, are specifically designed. Flex or bend sensors are commonly employed to monitor and track the deformation of soft bending actuators. These sensors are designed to detect and measure the degree of flexure or bending in the actuator, providing valuable feedback on its shape and movement.

The bending sensor's thickness and design (Fig. 1a) make its performance better during SPA movement, while the force sensor (Fig. 1b) maximizes contact with objects. The design process explores how the number of nodes affects their deformation, making them flexible for VTPU matrix integration, with evaluation based on area and node clearance. Sensors are designed with a 2 mm thickness for better flexibility and easy bending. The area of force sensor nodes is carefully determined to maximize object contact, aiming for compact volume and sufficient clearance between nodes to find out precise force and bending measurement. Computer aided design software is used for the initial actuator and sensor designs, as depicted in Fig. 1c. Additionally, Fig. 1d shows the 3D-printed SPA with sensors (method provided in the following section).

2.4 Fabrication

Resistive sensors offer a flexible and cost-effective means of monitoring SPAs, but their performance can be affected by continuous deformation and mechanical wear. To tackle this, a viable solution is to fabricate resistive sensors simultaneously with the actuator using a multi-material FDM printing approach. This integration within the actuator structure reduces the risk of mechanical damage, ensuring sensors remain functional during actuation.

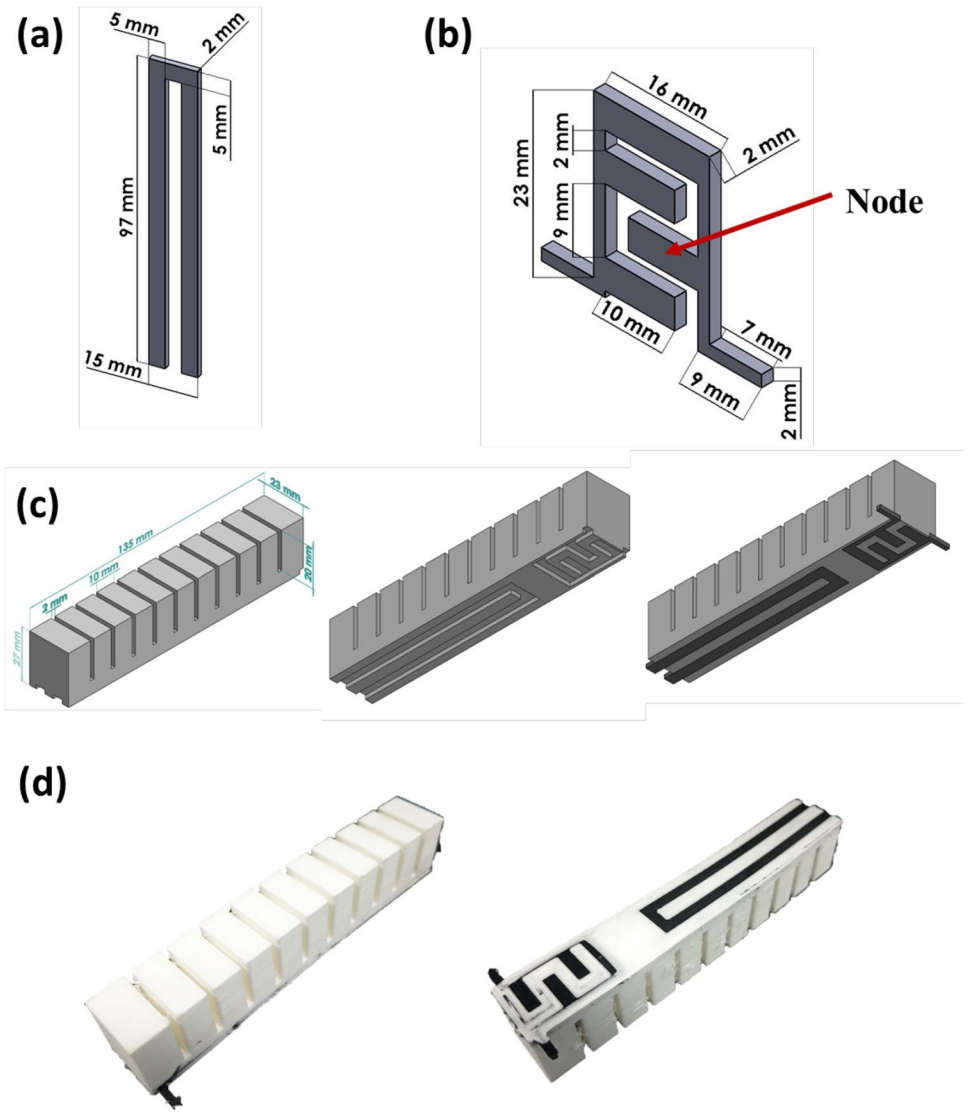

Fig. 1 Design and details of 3D-printed (**a**) soft bending sensor and (**b**) soft force sensor. Design and details of (**c**) SPA base and assembled SPA with embedded sensors. (**d**) 3D-printed SPA integrated with sensors

The samples are designed to be multi-material 3D printed without the need for support materials or post-processing techniques. Cura software is employed to slice the models, and the SPAs are then 3D printed using VTPU and CTPU on an Ultimaker S3 FDM 3D printer. The study utilizes optimal printing parameters, which are outlined in Table 1 and provided by the suppliers. To reduce material consumption during the printing process, additional support settings are not utilized. According to the previous study [35], the shore hardness of the material is determined to be 67 A when printed at a nozzle temperature of 220 °C. This specific printing temperature is selected for the VTPU during the experiment. The thickness of structures should be at least 1 mm to avoid material drop or poor binding. It should be noted, the actuator's bending ability is significantly influenced by gravity during fabrication. The supplier recommended setting the bed temperature to 0 °C which is equal to room temperature (25 °C) to achieve better results during the printing process.

For the simultaneous printing of the two materials, the printing settings are largely kept similar. To achieve high-quality design output, the infill patterns are adjusted to decrease printing issues arising from the use of multiple filaments. Additionally, the prints are oriented horizontally, with the largest surface in contact with the printing bed, to enhance stability during printing. Regular inspections are conducted throughout the printing process to eliminate printing errors and accomplish satisfactory results.

2.5 Control and measurement for SPA

SPAs are actuated using a Clarke air compressor (8 bar max working pressure). Airflow control is done through a basic gauge (pressure range: 100-300 kPa). Actuators are clamped horizontally, and data are recorded during the experiment. Resistance of sensors during deformation is measured with a Keithley 2110 digital multimeter. The Sauter FK100 force gauge measures the applied force on the force sensor. A timer is used to standardize the sequence of steps. These instruments played crucial roles in accurately monitoring and measuring pressure, resistance, and force in the experiment.

During the testing procedure, the engineering workbench LabVIEW is employed as a communication platform with the necessary instruments. A dedicated system as shown in Fig. 2a is developed to collect data periodically from the fabricated sensors. The force sensor used in the study is calibrated and measured using a Sauter FK100 force gauge. The calibration process involved applying various loads from 5 N to 15 N to the sensor and monitoring the corresponding changes in resistance (see Fig. 2b). By establishing the relationship between the applied loads and the sensor's resistance, the force sensor could accurately measure and quantify forces during the experimental testing. The Capstone software measures the bending angle of the SPAs by recording their movement during the experiment. The procedure of the testing plan for all materials and SPAs is shown in Fig. 2c. By analysing the recorded data, it accurately quantifies the actuator's bending behaviour based on the input pressure. The resistance and time data are collected during the actuating procedure. For result reliability, the experiment is repeated three more times, and the average resistance is calculated. This iterative process helps to validate the accuracy and consistency of the obtained resistance values. The relative resistance (R_{rel}) is calculated by $R_{rel} = \frac{R-R_0}{R_0}$ and determined by measuring the resistance of the sensor (R) and comparing it to the sensor's initial resistance (R_o).

2.6 Finite element analysis

In the simulation section, a pure mechanical analysis without sensing features is conducted. Testing in a single 3D printing orientation is chosen since stress-strain curves showed similar patterns in both longitudinal and transverse directions. The constitutive model fitting focuses on the material printed in the longitudinal orientation due to the predominant stresses occurring in that direction during actuation. The Yeoh model is found to accurately capture the elastic behaviour of the material across a wide range of strains [48]. In this study, the longitudinal data obtained from mechanical testing is fitted to Yeoh's hyper-elastic model. The experimental data during the mechanical testing, specifically in the strain range of 0-5, is successfully fitted using this model finite element method (FEM) (see Table 2).

The stress-strain data from the tensile test are used in the simulation. The data is imported into ANSYS® software, and a mesh convergence study is conducted repeatedly until reaching a tip force and bending angle that closely matches the experimental results. This allows for a comparison with 3D-printed actuators. The simulations focus on evaluating the structural behaviour and performance of the SPAs using static analysis. To mesh the models of the soft actuators, an adaptive meshing approach is employed using higher-order tetrahedral elements (10-node tetrahedral element) with a mesh size of 5 mm. The assumption is made that the material of the actuators is isotropic and incompressible. The density of the actuator material is specified as 1.2 g/cm^3. To accurately capture the behaviour of the actuators during deformation, surfaces that come into contact are identified and treated as frictional self-contact pairs. The contact behaviour is modified to be symmetric, aiming to lower penetration and achieve more realistic results.

The internal surfaces of the chambers within the actuators experience a maximum pressure of 300 kPa, while the base of the actuators has a fixed support boundary condition.

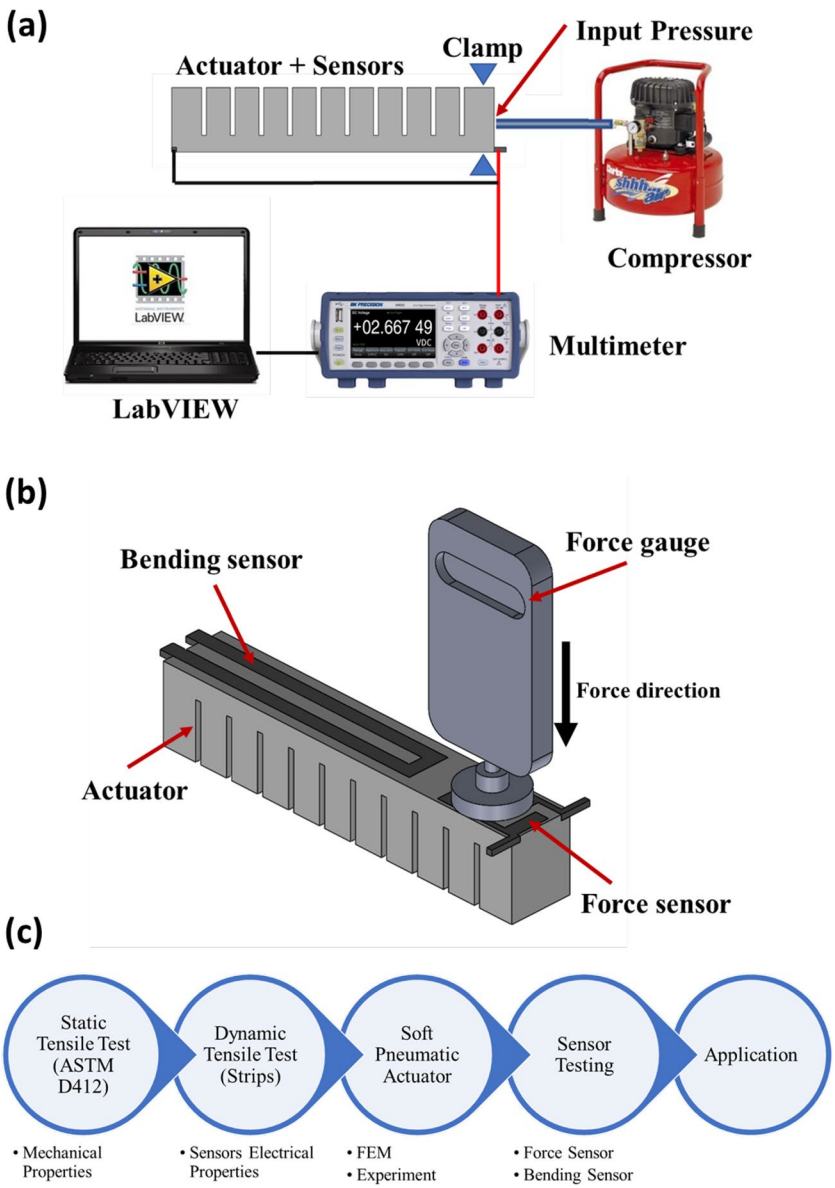

Fig. 2 (**a**) A schematic illustrating the configuration of the air control system incorporating both the force and bending sensors. (**b**) A diagram illustrating the procedure of force measurement. The force gauge is applied in a direction that maximizes the contact between the gauge and the force sensor, ensuring better interaction between the two. (**c**) Test plan for sensors and SPA

Gravity is taken into consideration to obtain more precise and realistic results. Solid tetrahedral quadratic hybrid elements are employed to simulate all components of the actuators. The proximal ends of the actuators are subjected to a fixed boundary condition, indicating that they are fixed in place. To enhance computational efficiency, the inlets of the actuators are not considered, and instead, air pressure is directly applied to the interior walls of the cavities within the actuators.

Table 2 Hyper-elastic models' strain energy function representation [49]

Model	Yeoh
Equation	$W = C_{10}(I_1 - 3) + C_{20}(I_1 - 3)^2 + C_{30}(I_1 - 3)^3$
Parameters	$C_{10} = 2.038$, $C_{20} = 0.039$, and $C_{30} = 0.00057$

W is the strain energy density function. C_{10}, C_{20}, and C_{30} are material-specific parameters, while I_1 is the first deviatoric strain invariant.

3 Results and discussion

3.1 Mechanical testing

To gain a deeper understanding of the mechanical properties, the VTPU and CTPU filaments undergo tensile tests. The tensile tests are conducted in accordance with the guidelines outlined in ASTM D412-16 with a controlled rate of 500 mm/min until samples break. Figure 3a illustrates the mechanical behaviour of VTPU and CTPU under the tensile test. Tests are repeated three times and average results are

presented accordingly. The tensile specimens are subjected to stretching until they reach failure. According to the findings, VTPU fractures after experiencing a strain of 300%, whereas CTPU fractures prior to reaching 300% strain. The elastic modulus and ultimate strength values obtained from the uniaxial tensile test for CTPU are approximately 31.3 MPa and 7.1 MPa, respectively. Similarly, for VTPU, the elastic modulus and ultimate strength are around 30.7 MPa and 6.07 MPa, respectively. Upon comparing the data, it becomes evident that CTPU typically exhibits a slightly greater elastic modulus and ultimate strength in comparison to VTPU. This disparity can be attributed to the lower shore hardness of VTPU in comparison to CTPU. All specimens initially exhibited elastic behaviour with the graph showing a linear trend at low strain levels (up to 5%). However, this linearity is disrupted, and a nonlinear curve emerged until the yield point is reached. Beyond the yield point, strain hardening behaviour is observed, resulting in significant deformation without necking until the breaking point.

CTPU onto VTPU strips with dimensions of 130 mm x 10 mm x 0.3 mm are printed to evaluate the mechanical and electrical properties of the sensor with the dynamic tensile test. In Fig. 3b, the result of the static tensile test is shown. Below 30% strain, there is an increase in the absolute

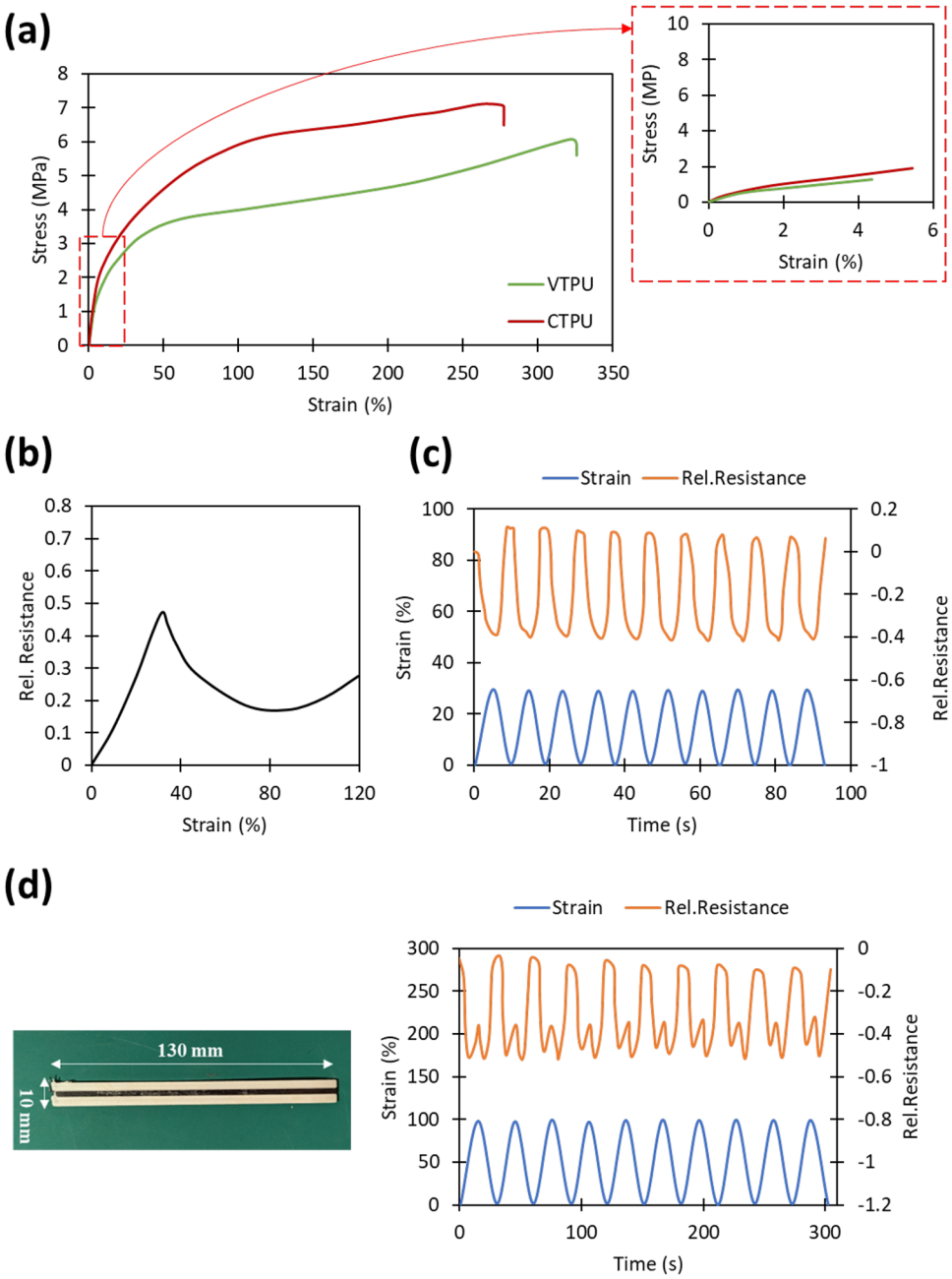

Fig. 3 (**a**) Static tensile tests' average results for VTPU and CTPU. The integrated strain CTPU within the VTPU strips provided sensor response data during (**b**) static tensile test (absolute value of resistance) and dynamic tensile testing across a range of (**c**) 0% to 30% strains and (**d**) 0% to 100% strains at a 200 mm/min rate

value of relative resistance. After this first rise, the relative resistance falls. Later, up to 120%, the relative resistance rises slightly. The relative resistance increases noticeably as the strain is raised all the way to the fracture point. Also, we assess the dynamic performance of these printed strips, which include integrated sensor components. The testing involves altering strain levels between 0% and 30% and 0% and 100% while keeping a constant speed of 200 mm/min. In Fig. 3c, the dynamic testing results are depicted for VTPU and CTPU combinations created using a multi-material FDM printer. When observing the sensor signal during the dynamic testing, it is evident that the relative resistance behaviour does not align with the applied strain. During the initial phase of the first cycle, as the strain increased up to 30%, the relative resistance subsequently decreased. There is an inverse relationship observed between the relative resistance and the strain. Specifically, as the strain increases, the relative resistance decreases, and conversely, when the strain decreases, the relative resistance increases.

In addition to the dynamic test conducts between 0% and 30% strains, dynamic tensile testing is also carried out over a broader range, specifically between 0% and 100% strains (see Fig. 3d). As the strain increases from 0% to 100%, there is an initial decrease followed by an increase in the sensor signal. However, it is worth noting that a plateau is observed in the sensor signal during this testing range. Compared to what was seen in the range of strains 0-30%, the uncertainty became apparent at higher strains. Due to a higher strain, resistance response changes throughout the strain range of 0 to 100%. As shown in Fig. 3b, resistance decreases after a strain of 30% and increases slightly after an 80% strain. This affects the result of dynamic tests in the range of 0% to 100%. When the strain is between 0 and 100%, the slope shifts from negative to positive, which leads to a secondary peak. However, the outcomes remain the same for the course of the dynamic tensile test. This behaviour suggests that the viscous component of the viscoelastic behaviour of the printed VTPU had a dominant influence on the mechanical and resistance characteristics, resulting in a higher degree of remaining deformation [47, 50].

The results of the study indicate that the integration of the CTPU sensor and VTPU matrix exhibits consistent changes in resistance, which can be highly valuable for SPAs. The resistance variations demonstrate a steady pattern during dynamic mechanical testing. This finding suggests that the integrated CTPU-VTPU system possesses responsive electrical properties that can be harnessed for sensing and actuation applications. The consistent changes in resistance provide a reliable means of detecting and monitoring the mechanical behaviour of the composite material. This is especially beneficial in dynamic environments where real-time feedback and control are crucial. The electrical response is governed by the viscoelastic properties of the printed TPU, with the viscous component playing a dominant role. This influences the mechanical and resistance behaviours, resulting in a higher degree of remnant deformation. The resistance curve shows linearity, except for the plateau caused by resistance changes, indicating potential for accurate and predictable sensing capabilities.

3.2 Bending behaviour

The SPAs are controlled by adjusting the air pressure applied to them. When air pressure is increased or decreased, the actuators bend accordingly. The SPA is powered by a compressor, which supplies the necessary air pressure. The VTPU material used in manufacturing the actuator allows for a range of bending degrees depending on the specific test conditions and parameters applied. Figures 4a and b depict the bending behaviour of the simple actuator as observed in both simulation and experimental results. The applied pressure ranges from 100 to 300 kPa for all the actuators. The results likely present a comparison between the predicted bending in the simulation and the actual bending observed in the experimental setup. The results demonstrate how the actuators move and deform in response to varying levels of applied pressure. The trajectories show the path taken by the actuators as they undergo bending and movement, providing insight into their behaviour under different pressure conditions. Through the analysis, it is observed that the FEM models accurately match the observed bending angles of the SPAs. The maximum difference between the predicted and observed bending angles is found to be 1.2% at 300 kPa. These small differences indicate a high level of agreement between the FEM models and the experimental results, demonstrating the accuracy of the simulation in predicting the bending behaviour of the SPAs. As the pressure is increased, it is observed that the bending sensor's behaviour changes as well.

In addition to the measurements, tests are performed by measuring the resistance of the sensor at different pressure levels. This approach provided an additional means of monitoring and analysing the behaviour of the sensor under varying pressure conditions. By observing the changes in resistance, valuable insights are gained regarding the sensor's response and its relationship with the applied pressure. The resistance of the flex sensor is measured using a multimeter starting from time 0 s. Immediately after, a pressure of 100 kPa is applied to the SPA. This pressure is maintained for 5 seconds before being released. Sufficient time (15 seconds) is given for the actuator to return to its neutral position by deflating. A 5-second delay followed, after which the subsequent pressure is applied. This entire process is repeated six more times. The procedure is then replicated for 200 kPa and 300 kPa pressures.

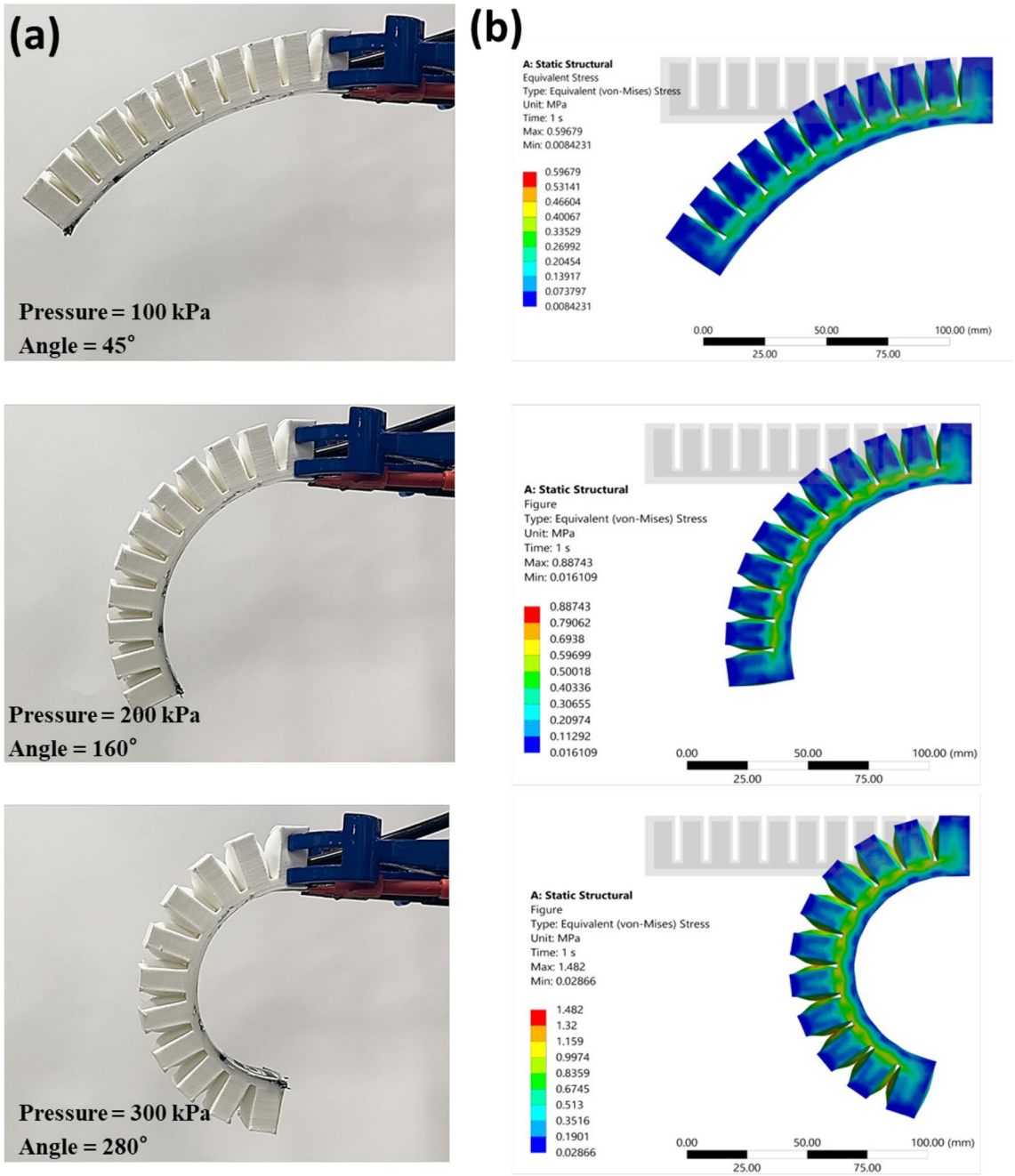

Fig. 4 A comparative analysis of the bending shape of a simple actuator can be observed in two scenarios: (**a**) experimental results and (**b**) simulation results at various pressure levels

Following the completion of the 3D printing process, the printed bending sensor is subjected to measurements of static resistance. The recorded data reveal an exponential decrease in resistance from an initial value of 14.48 kΩ to 14.36 kΩ over a period of 100 seconds after connecting the sensor to the multimeter. These findings can be attributed to the specific fabrication method employed, indicating a limited connection between the printed layers and the extruded material. The variations in adhesion between these layers could potentially introduce imbalances during the experimental procedure. To mitigate the potential impact of material influences on the testing process, a waiting period of 60 seconds is introduced to allow the resistance to stabilize and achieve greater consistency before conducting the experiments. Following the experiment, the raw data is plotted on an XY graph to observe the average resistance values corresponding to different pressure levels. For 100 kPa pressure, the average

resistance is measured at 13.50 kΩ or -0.02 relative resistance (see Fig. 5a). Similarly, the average resistance for 200 kPa pressure is found to be 12.86 kΩ or -0.07 relative resistance as shown in Fig. 5b, and for 300 kPa pressure, it is 12.45 kΩ or -0.1 relative resistance (see Fig. 5c). These average resistance values are presented indicating a certain level of consistency in the sensor readings. The data also reveals that after the pressure is released, there is a delay in the sensor reaching its resting point. This delay can be attributed to the actuator taking time to release the pressure, resulting in a lag in the sensor response.

Figure 5d clearly demonstrates a noticeable variation in resistance as the pressure increases. Due to the significant thickness of the design, the resistance changes observed in SPAs are not entirely constant. The variations in resistance can be attributed to factors such as the complex internal structure and the distribution of conductive elements within the SPAs. Additionally, it is worth noting that the SPAs do not fully recover their original state after being stimulated. This incomplete recovery can be attributed to various factors, including the viscoelastic nature of the material and the mechanical stresses experienced during operation. The viscoelastic behaviour of the materials causes both viscous flow and elastic deformation during inflation and deflation cycles, leading to irreversible changes in their structure over time. Additionally, repeated mechanical stresses and environmental factors contribute to material degradation, further affecting the actuator's ability to recover fully. By incorporating softer materials such as silicone and elastomer, it becomes possible to address the existing issue effectively,

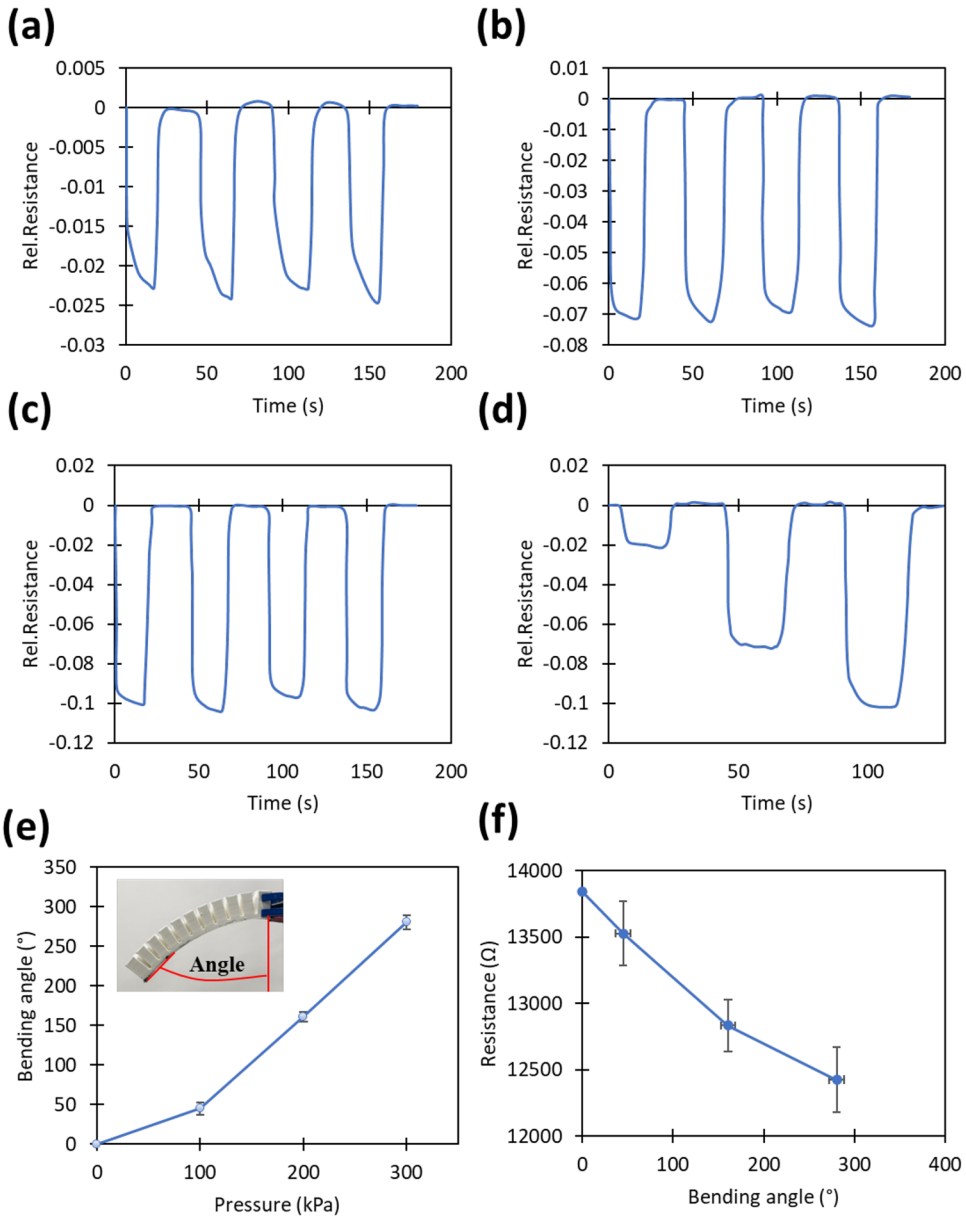

Fig. 5 The variations in relative resistance over time for SPAs operating under an input pressure of (**a**) 100 kPa, (**b**) 200 kPa, and (**c**) 300 kPa. (**d**) The changes in relative resistance over time for cumulative pressure applied to the SPA. (**e**) The measured bending angles of the SPA at different input pressure levels. (**d**) The relationship between resistance changes and the resulting bending angle of the SPA

thereby significantly enhancing the performance of SPAs. Furthermore, optimizing the design of SPAs can yield substantial benefits, leading to enhanced overall functionality. By carefully analysing and refining the structural layout, engineers can identify areas for improvement, fine-tune critical components, and ensure seamless interactions between various elements. This process of design optimization allows SPAs to operate more efficiently, delivering enhanced user experiences and elevating their capabilities to new heights.

The average resistance exhibits a substantial decrease from 100 kPa to 200 kPa. Furthermore, the average resistance continues to decrease from 200 kPa to 300 kPa. These observations indicate that the change in resistance exponentially decreases as greater pressure is applied. These findings confirm that the flex sensor effectively monitors the deformation of a SPA, as it accurately captures the changes in resistance corresponding to different pressure levels. Simultaneously, the bending angle of the SPAs is recorded and monitored throughout the experiment. As shown in Fig. 5e, results reveal that by increasing the pressure, the bending angle is also increased. Moreover, Fig. 5f illustrates a clear relationship between the applied pressure, the bending angle of SPAs, and the bending sensor's corresponding resistance reduction. As the pressure increases, it causes a proportional increase in the bending angle of the SPAs. This increase in bending angle is accompanied by a reduction in resistance detected by the bending sensor.

3.3 Blocked force behaviour

The blocked force is a critical performance parameter for soft actuators as it represents the force generated by the tip of the SPA. It demonstrates the actuator's capability to convert pressure into force effectively. The actuator is securely attached at one end and functions as a cantilever beam. As the input pressure increases, the output force of the actuator also rises accordingly. When measuring the force, the pressure is incrementally increased in steps of 100 kPa, reaching a maximum pressure of 300 kPa. When only a small amount of pressure is applied to the actuator, the bending angle is minimal, and the majority of the blocked force is generated by the weight of the actuator itself. However, as the input pressure increases to a sufficient level, the sensor starts to provide resistance to the bending actions of the actuator, resulting in an increase in the bending angle. In a similar manner to the flex sensor, the change in resistance of this sensor is examined by applying load manually using a Sauter FK 100 force gauge. The resistance change of the sensor is observed using a multimeter. The force is incrementally exerted in increments from 5 N to 15 N, with equal intervals between each cycle (see Fig. 6a). Each applied force is repeated three times to have accurate measurements.

When the actuator comes into contact with the sensor base, it bends into an arch shape. The top layer of the actuator expands and moves forward as it inflates. The increased blockage in this case can be attributed to the bending motions of the actuator and the contact with the sensor, which restricts the flow and increases the resistance. In ANSYS, a fixed support boundary condition is applied to the proximal end of the actuator during the blocked force simulations. This setup treats the actuator as a cantilever beam. The distal end of the actuator is assigned a displacement support condition, which allows it to slide without friction. This arrangement simulates a load cell and enables force measurements to be taken (see Fig. 6b). The displacement support in place resists the bending deformation of the soft actuator when it is pressurized. As a result, the actuator bends backwards, forming an arch shape, and slides along the displacement support. Figure 6c provides a summary of the blocked force data for the SPAs. It can be observed that as the pressure increases, the force exerted by the actuator also increases.

The SPA exhibits the highest force and actuation pressure of 3 N when subjected to a pressure of 300 kPa. The comparison between the simulated and measured force indicated a difference of 0.05 N, demonstrating the simulation's ability to accurately predict the blocked force. This technique can effectively achieve the required force, thereby reducing the need for additional effort. The bending and tip force outcomes of the SPAs align closely with the findings of previous research studies [35, 51, 52]. The successful performance of the actuator using VTPU material indicates that it functions effectively and achieves the desired outcomes. Nevertheless, by incorporating soft sensors internally, it becomes possible to control the bending and tip force of the pneumatic actuators more precisely. This implementation also leads to a reduction in material waste.

3.4 Applications

According to the experimental findings, the sensors demonstrate the capability to detect changes during deformation and when encountering an unknown force. The SPA can be effectively utilized as a soft gripper for handling delicate or foreign objects such as 3D-printed objects, oranges, and bananas. The functionality of the soft gripper is observed while successfully grasping items (see Fig. 7a). A pressure of 100 kPa is employed as the input to initiate the SPAs. The behaviour of the actuators is continuously monitored and controlled throughout the entire procedure. Once the actuators begin to bend and contact the objects, the LabVIEW system promptly initiates the monitoring process, capturing and recording any alterations in resistance (see Fig. 7b). It is observed that the displacement of the flex sensor remained

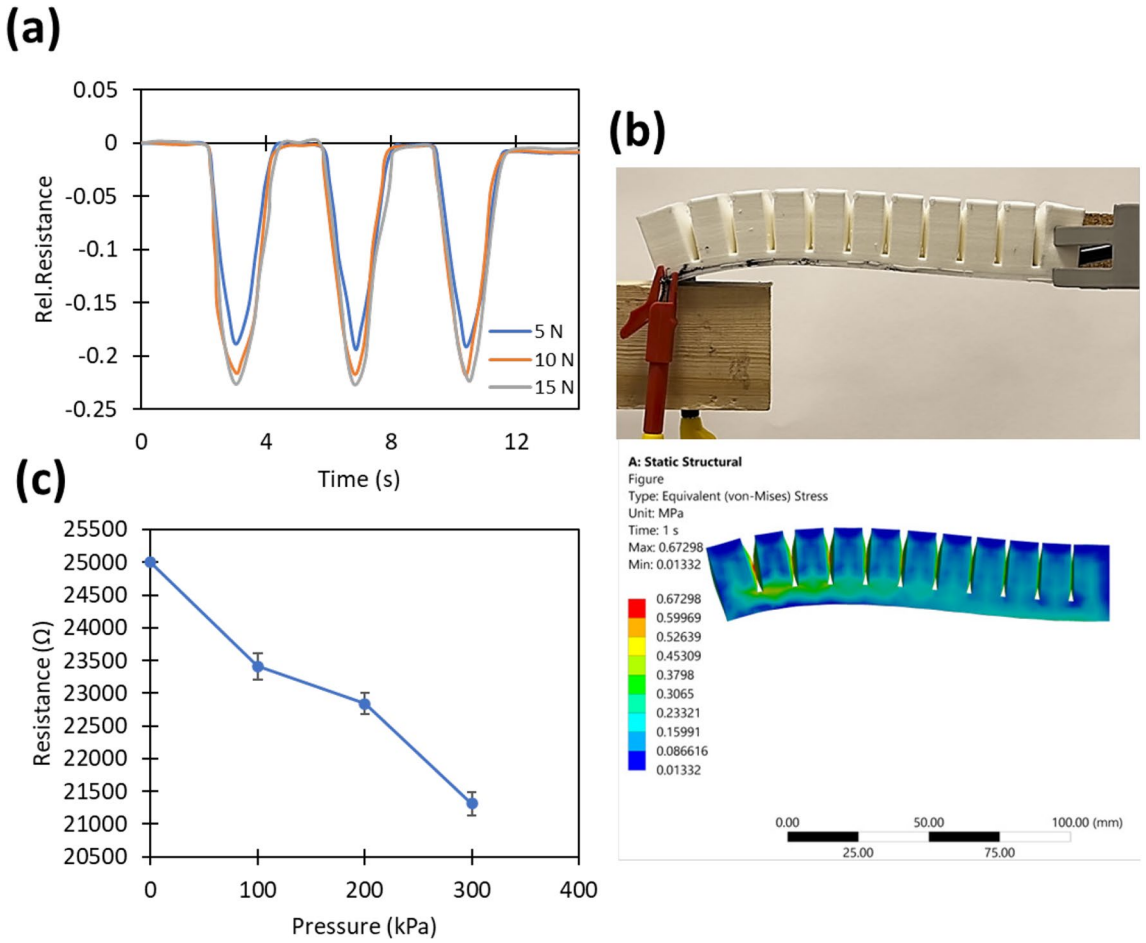

Fig. 6 (**a**) The obtained relative resistance values via the measurement and calibration of the force sensor using a force gauge. (**b**) The experimental and simulated results of the blocked force using a pressure of 100 kPa. (**c**) The relationship between resistance changes and the resulting blocked force of the SPA

constant after securing the objects in place, indicating that their presence does not affect the sensor's position. However, an alteration in resistance is detected as the pressure increased, indicating an increase in pressure when holding the object. The 2D SPAs exhibit the expected behaviour, with the fingers curling appropriately. The contact with the objects being grasped is limited to the tips of the fingers. Throughout the experiment, all parameters are maintained at a constant level. It is demonstrated that the inclusion of the metamaterial resulted in successful grasping, reaffirming its positive impact on the grasping capabilities.

The SPA demonstrates its versatility in the realm of rehabilitation gloves, offering valuable assistance to individuals recovering from hand impairments caused by accidents or other health conditions (See Fig. 7c). By incorporating five pneumatic bending actuators, these gloves provide targeted support to the client's hand. When pressure is applied, the actuators induce the closing motion of the hand, creating controlled resistance. To halt the glove from completely closing the hand, the client is encouraged to engage their motor receptors, promoting active participation in the rehabilitation process. To evaluate the progress made during rehabilitation, a sensor embedded within the glove accurately measures the displacement of the hand from its original position. This data enables healthcare professionals to assess the client's advancement and adjust the rehabilitation programme ensuring personalized and effective recovery. In addition to its rehabilitative function, the SPA glove also serves as an exoskeleton, offering supplementary assistance for forelimb locomotion. By providing external support and augmenting the user's movement, the glove aids individuals in regaining strength, coordination, and range of motion in their upper limbs. The SPA's application as a rehabilitation glove not only facilitates the recovery of hand impairments but also serves as an innovative tool for therapeutic interventions and improved functional outcomes in the field of rehabilitation medicine. The concept can be enhanced by refining the design to closely replicate the joint-segment,

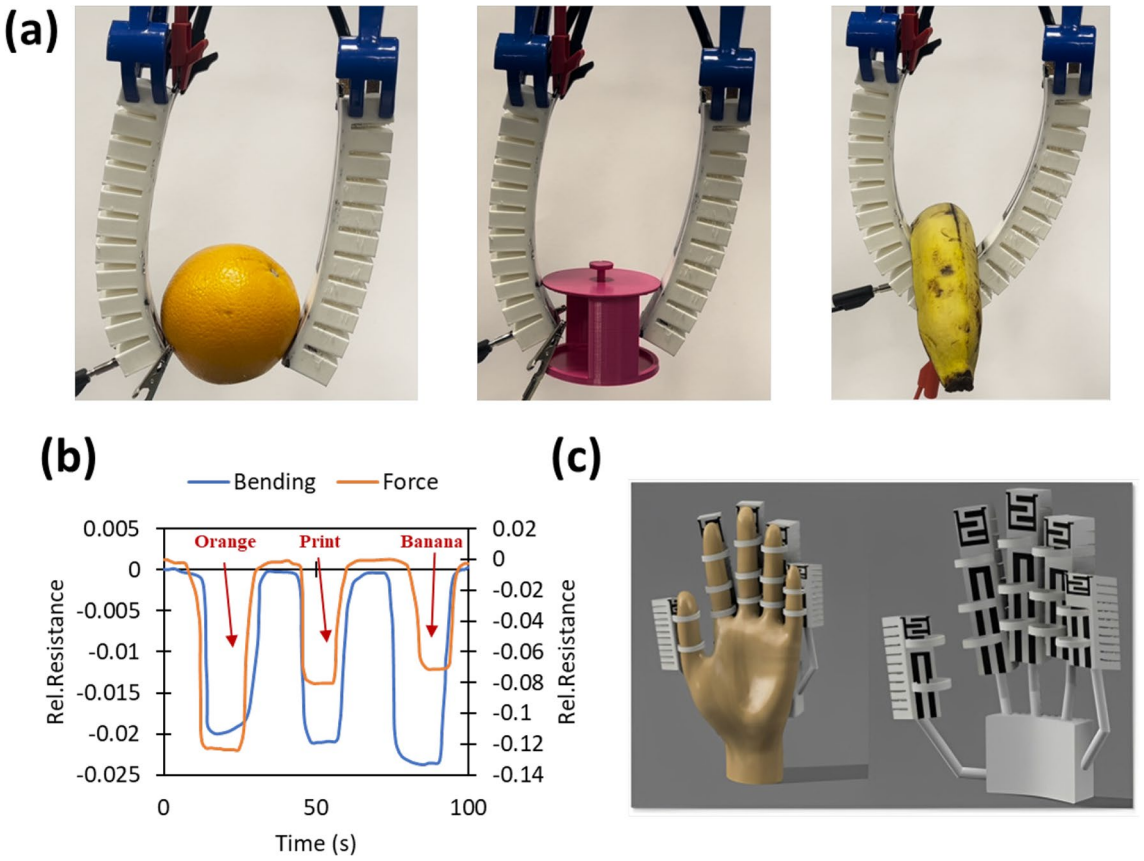

Fig. 7 (**a**) Captured images of a flexible robotic gripper successfully capturing various objects of diverse shapes and sizes. (**b**) The relative resistance readings from the two sensors as the gripper securely grasps objects. (**c**) The creation of 3D models concept representing actuators designed specifically for use as rehabilitative devices

resulting in superior functionality. This advancement should be a focus of future research efforts to assess the overall system's performance, encompassing vital aspects like sensor connections.

4 Conclusion and future work

This article introduces a novel category of SPAs with integrated soft sensors and fabricated using FDM 3D printing. The study includes simulations and successful 3D printing of the designed SPAs with specific material properties. Experiments show that the flex sensor accurately determines pressure levels (1.4 kΩ at 300 kPa) and calculates deformation angles in the soft actuator. The force sensor monitors forces (6 kΩ at 15 N) applied to the sensor. These sensors are integrated into soft grippers, demonstrating effective grasping of various objects. A conceptual design proposes their use as rehabilitative devices, offering promising potential for future research. Further studies can deepen the understanding of 3D-printed sensors integrated within soft actuators. Conducting additional experiments to assess sensor durability, such as creep testing and evaluating tensile stress and strain at the fused material's borders, would be valuable to determine the actuators' maximum stress levels. Exploring alternative materials like carbon nanotubes and conductive composites in combination with actuators could help assess their suitability and strength. Expanding the range of soft conductive filaments and testing their performance in various types of actuators would also broaden the research scope. By pursuing these studies, we could gain comprehensive insights into 3D-printed sensors in soft actuators, leading to advancements in the field and unlocking innovative applications.

Acknowledgements The authors would like to thank the 4D Materials and Printing Lab at Nottingham Trent University for providing software and hardware facilities for conducting this research.

Author Contributions Conceptual Design, Methodology: MLD and MB.
Data Collection, Validation: MLD and RS.
Writing—original draft, Visualization MLD.
Investigation, Formal Analysis, Writing—review & editing: MLD, RS, AZ, HYN, and MB.
Resources, Supervision: MB.

Funding The authors declare that no funds, grants, or other financial support were received during the preparation of this manuscript.

Declarations

Competing Interests The authors have no relevant financial or non-financial interests to disclose.

References

1. Xavier MS, Tawk CD, Zolfagharian A, Pinskier J, Howard D, Young T et al (2022) Soft pneumatic actuators: A review of design, fabrication, modeling, sensing, control and applications. https://doi.org/10.1109/ACCESS.2022.3179589
2. Zolfagharian A, Mahmud MAP, Gharaie S, Bodaghi M, Kouzani AZ, Kaynak A (2020) 3D/4D-printed bending-type soft pneumatic actuators: Fabrication, modelling, and control. Virtual Phys Prototyp 15 (4):373–402. https://doi.org/10.1080/17452759.2020.1795209
3. Walker J, Zidek T, Harbel C, Yoon S, Strickland FS, Kumar S et al (2020) Soft robotics: A review of recent developments of pneumatic soft actuators. Actuators 9(1):3. https://doi.org/10.3390/act9010003
4. Ni X, Liao C, Li Y, Zhang Z, Sun M, Chai H et al (2020) Experimental study of multi-stable morphing structures actuated by pneumatic actuation. Int J Adv Manuf Technol 108(4):1203–1216. https://doi.org/10.1007/s00170-020-05301-1
5. Lalegani Dezaki M, Bodaghi M (2023) A review of recent manufacturing technologies for sustainable soft actuators. Int J Precis Eng Manuf - Green Technol. https://doi.org/10.1007/s40684-023-00533-4
6. Li M, Pal A, Aghakhani A, Pena-Francesch A, Sitti M (2022) Soft actuators for real-world applications. Nature Rev Mater 7(3):235–249. https://doi.org/10.1038/s41578-021-00389-7
7. El-Atab N, Mishra RB, Al-Modaf F, Joharji L, Alsharif AA, Alamoudi H et al (2020) Soft actuators for soft robotic applications: A review. Adv Intell Syst 2(10):2000128. https://doi.org/10.1002/aisy.202000128
8. Jones TJ, Jambon-Puillet E, Marthelot J, Brun P (2021) Bubble casting soft robotics. Nature (London) 599(7884):229–233. https://doi.org/10.1038/s41586-021-04029-6
9. Zhao W, Wang Z, Zhang J, Wang X, Xu Y, Ding N et al (2021) Vat photopolymerization 3D printing of advanced soft sensors and actuators: From architecture to function. Adv Mater Technol 6(8):2001218. https://doi.org/10.1002/admt.202001218
10. Afshari P, Pavlyuk M, Lira C, Katnam KB, Bodaghi M, Yazdani Nezhad H (2023) Mechanical strain tailoring via magnetic field assisted 3D printing of iron particles embedded polymer nanocomposites. Macromol Mater Eng. https://doi.org/10.1002/mame.202300194
11. Khalid MY, Arif ZU, Ahmed W, Umer R, Zolfagharian A, Bodaghi M (2022) 4D printing: Technological developments in robotics applications. Sensors Actuators A Phys 343:113670. https://doi.org/10.1016/j.sna.2022.113670
12. Ji Q, Jansson J, Sjöberg M, Wang XV, Wang L, Feng L (2023) Design and calibration of 3D printed soft deformation sensors for soft actuator control. Mechatronics 92:102980. https://doi.org/10.1016/j.mechatronics.2023.102980
13. Won P, Kim KK, Kim H, Park JJ, Ha I, Shin J et al (2021) Transparent soft actuators/sensors and camouflage skins for imperceptible soft robotics. Adv Mater 33(19):2002397. https://doi.org/10.1002/adma.202002397
14. Lalegani Dezaki M, Bodaghi M (2023) Shape memory metalaminar jamming actuators fabricated by 4D printing. Soft Matter 19(12):2186–2223. https://doi.org/10.1039/d3sm00106g
15. Salifu S, Ogunbiyi O, Olubambi PA (2022) Potentials and challenges of additive manufacturing techniques in the fabrication of polymer composites. Int J Adv Manuf Technol 122(2):577–600. https://doi.org/10.1007/s00170-022-09976-6
16. Pearson C, Hawi S, Lira C, Goel S, Yazdani Nezhad H (2022) Magnetic field assisted 3D printing of short carbon fibre-reinforced polymer composites. Mater Today : Proc 64:1403–1411. https://doi.org/10.1016/j.matpr.2022.04.597
17. Daminabo SC, Goel S, Grammatikos SA, Nezhad HY, Thakur VK (2020) Fused deposition modeling-based additive manufacturing (3D printing): Techniques for polymer material systems. Mater Today Chem 16:100248. https://doi.org/10.1016/j.mtchem.2020.100248
18. Zhou J, Chen S, Wang Z (2017) A soft-robotic gripper with enhanced object adaptation and grasping reliability. https://doi.org/10.1109/LRA.2017.2716445
19. Manti M, Hassan T, Passetti G, D'Elia N, Laschi C, Cianchetti M (2015) A bioinspired soft robotic gripper for adaptable and effective grasping. Soft Robotics 2(3):107–116. https://doi.org/10.1089/soro.2015.0009
20. Yap HK, Ng HY, Yeow C (2016) High-force soft printable pneumatics for soft robotic applications. Soft Robotics 3(3):144–158. https://doi.org/10.1089/soro.2016.0030
21. Han K, Kim N, Shin D (2018) A novel soft pneumatic artificial muscle with high-contraction ratio. Soft Robotics 5(5):554–566. https://doi.org/10.1089/soro.2017.0114
22. Yeo JC, Yap HK, Xi W, Wang Z, Yeow C, Lim CT (2016) Flexible and stretchable strain sensing actuator for wearable soft robotic applications. Adv Mater Technol 1(3):1600018. https://doi.org/10.1002/admt.201600018
23. Shintake J, Cacucciolo V, Floreano D, Shea H (2018) Soft robotic grippers. Adv Mater 30(29):1707035. https://doi.org/10.1002/adma.201707035
24. Georgopoulou A, Egloff L, Vanderborght B, Clemens F (2021) A sensorized soft pneumatic actuator fabricated with extrusion-based additive manufacturing. Actuators 10(5):102. https://doi.org/10.3390/act10050102
25. Paterna M, De Benedictis C, Ferraresi C (2022) The research on soft pneumatic actuators in italy: Design solutions and applications. Actuators 11(11):328. https://doi.org/10.3390/act11110328
26. Georgopoulou A, Vanderborght B, Clemens F (2020) Multi-material 3D printing of thermoplastic elastomers for development of soft robotic structures with integrated sensor elements Zenodo. https://doi.org/10.5281/zenodo.5841572
27. Morrow J, Shin H-S, Phillips-Grafflin C, Jang S-H, Torrey J, Larkins R et al. (2016) Improving soft pneumatic actuator fingers through integration of soft sensors, position and force control, and rigid fingernails. Paper presented at the - 2016 IEEE International Conference on Robotics and Automation (ICRA), pp. 5024-5031. https://doi.org/10.1109/ICRA.2016.7487707

28. Stano G, Ovy SMAI, Edwards JR, Cianchetti M, Percoco G, Tadesse Y (2023) One-shot additive manufacturing of robotic finger with embedded sensing and actuation. Int J Adv Manuf Technol 124(1-2):467–485. https://doi.org/10.1007/s00170-022-10556-x
29. Mudhar R, Mucolli A, Ford J, Lira C, Yazdani Nezhad H (2022) Electrical and magnetic properties of 3D printed integrated conductive biodegradable polymer nanocomposites for sustainable electronics development. J Compos Sci 6(11):345. https://doi.org/10.3390/jcs6110345
30. Lotfian S, Giraudmaillet C, Yoosefinejad A, Thakur VK, Nezhad HY (2018) Electrospun piezoelectric polymer nanofiber layers for enabling in situ measurement in high-performance composite laminates. ACS Omega 3(8):8891–8902. https://doi.org/10.1021/acsomega.8b00940
31. Yap YL, Sing SL, Yeong WY (2020) A review of 3D printing processes and materials for soft robotics. Rapid Prototyp J 26(8):1345–1361. https://doi.org/10.1108/RPJ-11-2019-0302
32. Tawk C, Alici G (2021) A review of 3D-printable soft pneumatic actuators and sensors: Research challenges and opportunities. Adv Intell Syst 3(6):2000223. https://doi.org/10.1002/aisy.202000223
33. Tawk C, Mutlu R, Alici G (2022) A 3D printed modular soft gripper integrated with metamaterials for conformal grasping. Front Robot AI 8:799230. https://doi.org/10.3389/frobt.2021.799230
34. Cheng J, Wang R, Sun Z, Liu Q, He X, Li H et al (2022) Centrifugal multimaterial 3D printing of multifunctional heterogeneous objects. Nat Commun 13(1):7931. https://doi.org/10.1038/s41467-022-35622-6
35. Lalegani Dezaki M, Bodaghi M, Serjouei A, Afazov S, Zolfagharian A (2023) Soft pneumatic actuators with controllable stiffness by bio-inspired lattice chambers and fused deposition modeling 3D printing. Adv Eng Mater 25(6):2200797. https://doi.org/10.1002/adem.202200797
36. Damanpack AR, Sousa A, Bodaghi M (2021) Porous PLAs with controllable density by FDM 3D printing and chemical foaming agent. Micromachines (Basel) 12(8):866. https://doi.org/10.3390/mi12080866
37. Gariya N, Kumar P, Prasad B, Singh T (2023) Soft pneumatic actuator with an embedded flexible polymeric piezoelectric membrane for sensing bending deformation. Mater Today Commun 35. https://doi.org/10.1016/j.mtcomm.2023.105910
38. Hohimer CJ, Petrossian G, Ameli A, Mo C, Pötschke P (2020) 3D printed conductive thermoplastic polyurethane/carbon nanotube composites for capacitive and piezoresistive sensing in soft pneumatic actuators. Additive Manuf 34:101281. https://doi.org/10.1016/j.addma.2020.101281
39. Sonar HA, Gerratt AP, Lacour SP, Paik J (2020) Closed-loop haptic feedback control using a self-sensing soft pneumatic actuator skin. Soft Robotics 7(1):22–29. https://doi.org/10.1089/soro.2019.0013
40. Farrow N, Correll N (2015) A soft pneumatic actuator that can sense grasp and touch. Paper presented at the - 2015 IEEE/RSJ International Conference on Intelligent Robots and Systems (IROS), pp. 2317-2323. https://doi.org/10.1109/IROS.2015.7353689
41. Jung J, Park M, Kim D, Park Y-L (2020) Optically sensorized elastomer air chamber for proprioceptive sensing of soft pneumatic actuators. https://doi.org/10.1109/LRA.2020.2970984
42. Aloqalaa Z (2022) Electrically conductive fused deposition modeling filaments: Current status and medical applications. Crystals (Basel) 12(8):1055. https://doi.org/10.3390/cryst12081055
43. Yang H, Leow WR, Chen X (2018) 3D printing of flexible electronic devices. Small Methods 2(1):1700259. https://doi.org/10.1002/smtd.201700259
44. ColorFabb. VarioShore TPU natural. https://colorfabb.com/varioshore-tpu-natural
45. RECREUS INDUSTRIES S.L.™. Conductive filaflex material. https://recreus.com/gb/filaments/3-filaflex-conductivo.html
46. ASTM International (2014) Standard test method for tensile properties of plastics. https://doi.org/10.1520/D0638-14
47. Georgopoulou A, Sebastian T, Clemens F (2020) Thermoplastic elastomer composite filaments for strain sensing applications extruded with a fused deposition modelling 3D printer. Flex Print Electron 5(3):35002. https://doi.org/10.1088/2058-8585/ab9a22
48. YEOH, O. H. (1993) Some forms of the strain energy function for rubber. Rubber Chem Technol 66(5):754–771. https://doi.org/10.5254/1.3538343
49. Marechal L, Balland P, Lindenroth L, Petrou F, Kontovounisios C, Bello F (2021) Toward a common framework and database of materials for soft robotics. Soft Robotics 8(3):284–297. https://doi.org/10.1089/soro.2019.0115
50. Flandin L, Hiltner A, Baer E (2001) Interrelationships between electrical and mechanical properties of a carbon black-filled ethylene–octene elastomer. Polymer (Guilford) 42(2):827–838. https://doi.org/10.1016/S0032-3861(00)00324-4
51. Moseley P, Florez JM, Sonar HA, Agarwal G, Curtin W, Paik J (2016) Modeling, design, and development of soft pneumatic actuators with finite element method. Adv Eng Mater 18(6):978–988. https://doi.org/10.1002/adem.201500503
52. Huang W, Xu Z, Xiao J, Hu W, Huang H, Zhou F (2020) Multimodal soft robot for complex environments using bionic omnidirectional bending actuator. https://doi.org/10.1109/ACCESS.2020.3032983